Crack propagation monitoring in a full-scale aircraft fatigue test based on guided wave-Gaussian mixture model

2016 Smart Mater. Struct. 25 055048

(http://iopscience.iop.org/0964-1726/25/5/055048)

IOP Publishing Smart Materials and Structures
Smart Mater. Struct. **25** (2016) 055048 (13pp) doi:10.1088/0964-1726/25/5/055048

Crack propagation monitoring in a full-scale aircraft fatigue test based on guided wave-Gaussian mixture model

Lei Qiu, Shenfang Yuan, Qiao Bao, Hanfei Mei and Yuanqiang Ren

State Key Laboratory of Mechanics and Control of Mechanical Structures, Nanjing University of Aeronautics and Astronautics, 29 Yudao Street, Nanjing 210016, People's Republic of China

E-mail: ysf@nuaa.edu.cn

Received 16 November 2015, revised 1 March 2016
Accepted for publication 23 March 2016
Published 20 April 2016

Abstract

For aerospace application of structural health monitoring (SHM) technology, the problem of reliable damage monitoring under time-varying conditions must be addressed and the SHM technology has to be fully validated on real aircraft structures under realistic load conditions on ground before it can reach the status of flight test. In this paper, the guided wave (GW) based SHM method is applied to a full-scale aircraft fatigue test which is one of the most similar test status to the flight test. To deal with the time-varying problem, a GW-Gaussian mixture model (GW-GMM) is proposed. The probability characteristic of GW features, which is introduced by time-varying conditions is modeled by GW-GMM. The weak cumulative variation trend of the crack propagation, which is mixed in time-varying influence can be tracked by the GW-GMM migration during on-line damage monitoring process. A best match based Kullback–Leibler divergence is proposed to measure the GW-GMM migration degree to reveal the crack propagation. The method is validated in the full-scale aircraft fatigue test. The validation results indicate that the reliable crack propagation monitoring of the left landing gear spar and the right wing panel under realistic load conditions are achieved.

Keywords: structural health monitoring, full-scale aircraft fatigue test, crack propagation monitoring, time-varying condition, guided wave, Gaussian mixture model

(Some figures may appear in colour only in the online journal)

1. Introduction

Prognostics and health management (PHM) is an important technology to ensure the safety and to reduce the maintenance costs of aerospace vehicles [1, 2]. Structural health monitoring (SHM) is regarded to be a key technology of PHM and it has gradually developed from theoretic and fundamental research to real-world engineering application in recent decade. However, the following two key issues must be addressed for aerospace application [3–6].

The first key issue is the problem of reliable damage evaluation under aircraft in-service conditions because there are a lot of time-varying factors such as environmental temperature and humidity, random dynamic load and vibration, changing structural boundary condition, aerodynamic noise, engine noise, etc. These time-varying factors can introduce serious uncertain influence to SHM sensor signals to lead to the difficulty of reliable damage evaluation [3, 7, 8]. Several literatures have been published to deal with this issue, such as the method of environmental parameter compensation [9, 10], the method of baseline dependency reduction [11, 12], data normalization method [13], cointegration method [14], etc. However, these methods presented still cannot fully address the time-varying problem. In recent years, Gaussian mixture model (GMM) has been introduced to fault diagnosis of mechanical system [15–17] because it is an effective probability and statistics tool for characterizing uncertainties of sensor signals. Several initial researches began to introduce the GMM to the field of SHM. Tschöpe *et al* [18] reported the validation of using GMM for damage

degree classification on plate-like structure. Banerjee *et al* [19] adopted GMM to classify crack length of a plate-like repaired composite specimen. The sudden change of the environmental temperature was considered as a time-varying factor in the validation of this method but it is a simple situation. Yuan *et al* [20] proposed a GMM method to monitor a progressive damage on-line without using any mechanics model. The method was validated on a wing spar of a real aircraft under changing structural boundary condition in laboratory. Chakraborty *et al* [21] proposed a Dirichlet process GMM method combined with a mechanics model of crack to realize crack propagation monitoring of aluminum specimen under tensile fatigue load. However, the accurate mechanics model is difficult to be obtained and the load conditions are much more complicated in aerospace application. All these researches have proved the potential to apply the GMM to deal with the time-varying problem. However, deep research still needs to be performed with respect to the GMM for damage evaluation and their validation under real application situation.

The second key issue is that the SHM technology has to be fully validated on real aircraft structures under realistic load conditions on ground before it can finally reach the status of flight test, especially for the aerospace application which has strict limitation on new technology [3, 5, 6]. Nevertheless most of the SHM methods were only validated on small-scale structures in laboratory conditions. The full-scale aircraft fatigue test is one of the most similar test status to the flight test. The monitored structure is a real full-scale structure with complex geometry and connection. The dynamic fatigue load is complicated and it is obtained by using in-service flight data to simulate different flight modes of the aircraft such as takeoff, level flight, overloading, landing, on-ground etc. Hence, the damage evaluation is much more complicated than those validations performed on small-scale structures. Recently, Airbus reported their SHM validation in a full-scale aircraft fatigue test of A380 [3]. However there was few report on the validation process and results. In the validation carried out by Dragan *et al* [22] in a full-scale fatigue test of a military trainer aircraft, the crack states defined as 0–20 mm, 20–60 mm and >60 mm crack length were classified. However time-varying conditions were not taken into account and the sensor signals were acquired when the structure was in the static state. In addition, the crack monitoring sensitivity was low.

In this paper, the Guided Wave (GW) based SHM method [23–36] which has been studied widely due to high damage sensitivity, long detection range and on-line monitoring capability, is applied to a full-scale aircraft fatigue test to monitor the crack propagation under realistic load conditions. As mentioned above, the GW signals can be greatly influenced by time-varying conditions existed in aerospace application. To enhance the reliability of crack propagation monitoring under time-vary conditions, especially at the early stage of the crack propagation, a GW-GMM is proposed. The weak cumulative variation trend of the crack propagation mixed in time-varying influence can be tracked through GW-GMM modeling and on-line GW-GMM migration. Combining with a best match based Kullback–Leibler (KL) divergence, the migration degree of the GW-GMM can be quantified to reveal and evaluate the crack propagation. Based on this method, the crack propagations of the right landing gear spar and the left wing panel in the full-scale aircraft fatigue test are monitored reliably under realistic load conditions.

This paper is organized as follows. Section 2 proposes the GW-GMM including the damage monitoring principle, the on-line migration method and the migration measuring method. The implementation process of the GW-GMM is summarized as well. In section 3, the full-scale aircraft fatigue test is introduced and the GW signals acquired under fatigue load conditions are given and discussed. In section 4, the reliable crack propagation monitoring is realized by the GW-GMM. The GW-GMM construction and migration, and the crack propagation monitoring results are given. Finally, the conclusion is made in section 5.

2. guided wave-Gaussian mixture model

In this section, the damage evaluation principle of the GW-GMM is described first. Then, an on-line migration mechanism of the GW-GMM is proposed. After that, a GW-GMM migration index (MI) is defined to evaluate damage. Finally, the implementation process of the GW-GMM is summarized.

2.1. Damage monitoring principle of the GW-GMM

The GW signals acquired under time-varying conditions can be considered as a mixture of uncertain changes. Consequently, a GW feature can be considered as a random variable. Let $\mathbf{F} = \{\boldsymbol{F}_1,\ldots, \boldsymbol{F}_r,\ldots, \boldsymbol{F}_K\}$ be a GW feature sample set composed by K independent features which are obtained from K GW signals. $\boldsymbol{F}_r$ denotes a d-dimensional feature in the sample set, where $\boldsymbol{F}_r = [DI_1, DI_2,.., DI_d]^T$ and $r = 1, 2,\ldots, K$. When a monitored structure is in the healthy state, the GW feature sample set only contains the uncertain influence introduced by time-varying conditions. Under this situation, the feature sample set can be regarded as a GW baseline feature sample set.

Generally speaking, the sample set follows a joint probability density function (PDF) Φ which is unknown beforehand because of the complicated influence introduced by time-varying conditions. However, it still can be decomposed to be a mixture probability structure, just like that a signal can be decomposed to be a finite sum of signal components by using Fourier transform and wavelet transform. Therefore, the joint PDF of the GW feature sample set can be approximately modeled by a GMM which is considered as a finite weighted sum of Gaussian components Φ_i. The GMM is expressed as equation (1)

$$\Phi(\boldsymbol{F}_r \mid \boldsymbol{\mu}, \boldsymbol{\Sigma}) = \sum_{i=1}^{C} w_i \Phi_i(\boldsymbol{F}_r \mid \boldsymbol{\mu}_i, \boldsymbol{\Sigma}_i), \tag{1}$$

where C is the number of Gaussian components, $I = 1, 2,\ldots, C$. $\boldsymbol{\mu}_i$, $\sum_i$ and w_i are the mean, the covariance matrix and the

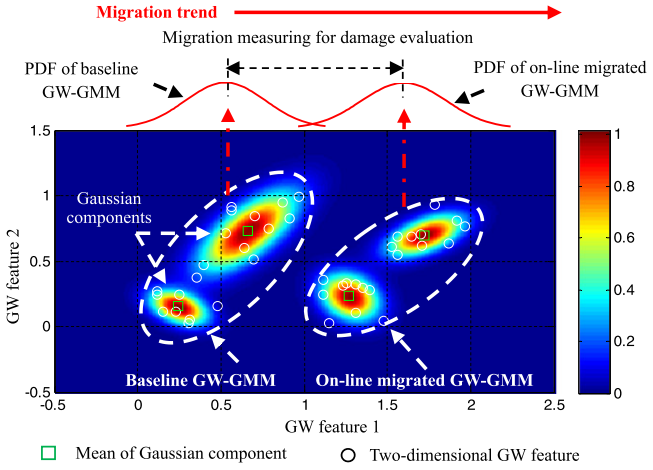

Figure 1. An example of the guided wave-Gaussian mixture model (GW-GMM).

mixture weight of the *i*th Gaussian component. The PDF of each Gaussian component is a *d*-dimensional Gaussian function which is expressed as equation (2)

$$\Phi_i(\boldsymbol{F}_r\,|\boldsymbol{\mu}_i,\,\boldsymbol{\Sigma}_i) = \frac{1}{(2\pi)^{\frac{d}{2}}|\boldsymbol{\Sigma}_i|^{\frac{1}{2}}} e^{-\frac{1}{2}(\boldsymbol{F}_r-\boldsymbol{\mu}_i)^T\boldsymbol{\Sigma}_i^{-1}(\boldsymbol{F}_r-\boldsymbol{\mu}_i)}. \quad (2)$$

The value of $\boldsymbol{\mu}_i$, $\sum_i$ and w_i can be obtained based on the sample set by using expectation maximization (*E–M*) algorithm [37, 38], in which, the initial value of $\boldsymbol{\mu}_i$, $\sum_i$ and w_i are acquired by using *k*-means clustering algorithm, and then a *E*-step and a *M*-step are performed iteratively to get the optimized value of $\boldsymbol{\mu}_i$, $\sum_i$ and w_i.

An example of a two-dimensional baseline GW-GMM composed of two Gaussian components is shown in figure 1, in which the GW-GMM is represented as a Nebula image. Each Nebula stands for a Gaussian component and the color stands for the two-dimensional probability density. The probability density of each Gaussian component is normalized independently.

When a new GW feature is obtained during an on-line damage monitoring process under time-varying conditions, a migration method can be adopted to rebuild the GW-GMM. Once the on-line migrated GW-GMM is obtained as shown in figure 1, some measuring methods of probability distribution difference can be adopted to quantify the migration between the on-line migrated GW-GMM and the baseline GW-GMM. This on-line migrating process can be performed continuously accompanying with the damage monitoring process. If the monitored structure keeps healthy, the result of migration measuring will be random and it will be maintained at lower level. If damage occurs in the structure and propagates continuously, a cumulative migration trend will be appeared in both the GW-GMM and the migration measuring result. Based on the result of migration measuring, the reliable damage monitoring can be realized.

2.2. On-line migration method of the GW-GMM

Based on the principle given above, the on-line migrating of the GW-GMM includes two steps. The first step is to update the GW feature sample set and the second step is to migrate the GW-GMM based on the updated feature sample set.

Ordinarily speaking, damage propagation such as crack is a slow and cumulative process. The damage induced variation on GW feature should be small when the damage is at early stage and the migration trend of the GW-GMM is weak. However, the GW feature which contains damage influence can be accumulated to enhance the migration trend of the GW-GMM. Therefore, to increase the on-line migration efficiency, the GW feature sample set is considered to be a queue sample set which means that it is updated based on the rule of first-in/first-out. An on-line MI is denoted as n ($n \geqslant 1$). When a new feature $\boldsymbol{F}^n$ is obtained, it is added to the sample set as the newest element. Meanwhile, the oldest element is moved out. The length of the sample set $\mathbf{F}^n$ is maintained to be K.

To increase the on-line migration efficiency of the GW-GMM, an improved *E–M* algorithm is proposed considering the slow cumulative property of the damage. As mentioned before, the baseline GW-GMM denoted as Φ^0 is constructed by the ordinary *E–M* algorithm and the initiation method is *k*-means clustering algorithm. However, in the improved *E–M* algorithm for on-line migration of the GW-GMM Φ^n, the PDF of the previous GW-GMM Φ^{n-1} is considered as the initial PDF of Φ^n. Then the *E*-step and an improved *M*-step are performed iteratively.

In *E*-step, the posteriori probability of a GW feature in each Gaussian component is calculated based on equation (3).

In *M*-step, w_i and $\boldsymbol{\mu}_i$ are updated based on equations (4) and (5) respectively. Then $\sum_i$ is updated. Considering that the likelihood value of the GW-GMM is a key to iteration stop criterion and the global maximum of the likelihood is corresponded to singular solutions with zero covariance [39], the *E–M* iteration step may converge to the singular solutions. To avoid this situation and keep the migration stably, $\sum_i$ is updated based on equation (6), in which, $\mathbf{I}_d$ is a *d*-dimensional unit matrix and $\boldsymbol{\alpha}$ is a correction factor which is determined according to the scale of the GW feature

$$P_{ri}(\boldsymbol{F}_r\,|\boldsymbol{\mu}_i,\,\boldsymbol{\Sigma}_i) = \frac{w_i\Phi_i(\boldsymbol{F}_r\,|\boldsymbol{\mu}_i,\,\boldsymbol{\Sigma}_i)}{\sum_{j=1}^{C} w_j\Phi_j(\boldsymbol{F}_r\,|\boldsymbol{\mu}_j,\,\boldsymbol{\Sigma}_j)}, \quad (3)$$

$$w_i = \frac{1}{K}\sum_{r=1}^{K} P_{ri}(\boldsymbol{F}_r\,|\boldsymbol{\mu}_i,\,\boldsymbol{\Sigma}_i), \quad (4)$$

$$\boldsymbol{\mu}_i = \frac{\sum_{r=1}^{K}[P_{ri}(\boldsymbol{F}_r\,|\boldsymbol{\mu}_i,\,\boldsymbol{\Sigma}_i)\boldsymbol{F}]}{\sum_{r=1}^{K} P_{ri}(\boldsymbol{F}_r\,|\boldsymbol{\mu}_i,\,\boldsymbol{\Sigma}_i)}, \quad (5)$$

$$\boldsymbol{\Sigma}_i = \frac{\sum_{r=1}^{K}[P_{ri}(\boldsymbol{F}_r\,|\boldsymbol{\mu}_i,\,\boldsymbol{\Sigma}_i)(\boldsymbol{F}_r-\boldsymbol{\mu}_i)(\boldsymbol{F}_r-\boldsymbol{\mu}_i)^T] + \alpha\mathbf{I}_d}{\sum_{r=1}^{K} P_{ri}(\boldsymbol{F}_r\,|\boldsymbol{\mu}_i,\,\boldsymbol{\Sigma}_i) + 1}. \quad (6)$$

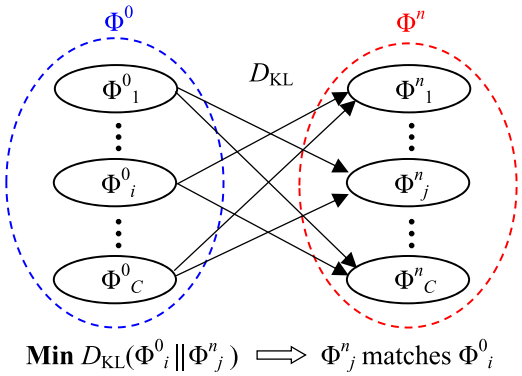

Figure 2. Illustration of the best match Gaussian components.

For stop determination of the *E–M* iteration, the log-likelihood value of the GW-GMM is used and the value is calculated based on equation (7). Supposing that the log-likelihood value at previous iteration step is L_0 and the log-likelihood value at current step is L_1, the *E–M* iteration is stopped if the convergence criterion shown in equation (8) is satisfied. If not, the iteration is performed continuously when the maximum iteration steps is reached. The value of ε is set to be 1×10^{-10}

$$L(\mathbf{F} \mid \Phi) = \sum_{r=1}^{K} \log \left[\sum_{i=1}^{C} w_i \Phi_i(\boldsymbol{F}_r \mid \boldsymbol{\mu}_i, \boldsymbol{\Sigma}_i) \right], \tag{7}$$

$$|L_1/L_0| - 1 < \varepsilon. \tag{8}$$

2.3. Migration measuring of the GW-GMM

The migration measuring result between the on-line migrated GW-GMM and the baseline GW-GMM is defined as MI. As mentioned before, the slow cumulative property of the damage will make the two GW-GMMs be overlapped together at the early stage of the crack propagation. However, accompanying with the damage propagation, the two GW-GMMs will be separated gradually. Considering the two conditions, a best match Gaussian component based KL divergence is proposed to calculate the MI and it is described as follows.

The KL divergence between two Gaussian components denoted as $\Phi^0{}_i$ and $\Phi^n{}_j$ can be calculated based on equation (9) [40]

$$D_{\mathrm{KL}}(\Phi_i^0 || \Phi_j^n) = \frac{1}{2}\mathrm{tr}[(\boldsymbol{\Sigma}_j^n)^{-1}(\boldsymbol{\Sigma}_i^0)] - \frac{d}{2} - \frac{1}{2}\ln\left(\frac{\det \boldsymbol{\Sigma}_j^n}{\det \boldsymbol{\Sigma}_i^0}\right) + \frac{1}{2}(\boldsymbol{\mu}_j^n - \boldsymbol{\mu}_i^0)^T(\boldsymbol{\Sigma}_j^n)^{-1}(\boldsymbol{\mu}_j^n - \boldsymbol{\mu}_i^0), \tag{9}$$

where $\boldsymbol{\mu}^0{}_i$, $\boldsymbol{\Sigma}^0{}_i$ and $w^0{}_i$ are the mean, the covariance matrix and the mixture weight of the *i*th Gaussian component of Φ^0. $\boldsymbol{\mu}^n{}_j$, $\boldsymbol{\Sigma}^n{}_j$ and $w^n{}_j$ are that of the *j*th Gaussian component of Φ^n. tr is the matrix trace and det is the determinant value.

As shown in figure 2, for each Gaussian component $\Phi^0{}_i$ in Φ^0, the KL divergence between it and all the Gaussian components in Φ^n is calculated first based on equation (9). If the smallest KL divergence happens between $\Phi^0{}_i$ and $\Phi^n{}_j$. It can be said that the best match Gaussian component of $\Phi^0{}_i$ in Φ^n is $\Phi^n{}_j$. Based on this point, the best match Gaussian component in Φ^n of each Gaussian component of Φ^0 can be found. Finally, the best match based KL divergence is calculated based on equation (10)

$$D_{\mathrm{KL}}(\Phi^0 || \Phi^n) = \sum_{i=1}^{C} w_i \min_j \left(D_{\mathrm{KL}}(\Phi_i^0 || \Phi_j^n) + \ln \frac{w_i}{w_j} \right). \tag{10}$$

2.4. Implementation process of the GW-GMM

The implementation process of the GW-GMM is summarized as figure 3 which includes two parts. The first part is the baseline GW-GMM construction. At this part, GW signals are acquired under time-varying conditions when the structure is in the healthy state, and GW features are extracted to construct a GW baseline sample set. After that, a baseline GW-GMM is constructed by the *E–M* algorithm with the initialization method of *k*-means clustering algorithm. The GW feature used in this paper are the time domain cross-correlation and the spectrum magnitude difference which will be given in the next section. The second part is the on-line GW-GMM for damage monitoring. At this part when a new GW signal is acquired, its feature is extracted first. Then the GW-GMM is migrated based on the queue sample rule and the improved *E–M* algorithm. When the PDF of the migrated GW-GMM is obtained, the MI is calculated. Finally, damage evaluation can be achieved according to the variation trend of the MI.

3. The full-scale aircraft fatigue test and GW signals

In this section, the full-scale fatigue test is introduced first. Then the uncertain influence of the time-varying conditions is discussed. After that, the crack propagation monitoring results based on damage index (DI) are given and discussed.

3.1. The full-scale aircraft fatigue test

The full-scale aircraft fatigue test was performed on an aircraft that had accumulated thousands of flight hours in China. One object of the fatigue test was to validate the GW based SHM system including the reliability of the PZT layer [41] under high fatigue strain level, the stability of the GW multi-channel scanning system [42] under on-line continuous working status and the capability of crack monitoring. The fatigue load was introduced by a series of force-controlled hydraulic loading devices and lever systems. The random dynamic fatigue load spectrum was generated by using the in-service flight data to simulate different flight modes of the aircraft. Prior to the start of the fatigue test, a set of commissioning load cases were applied to verify the correct functioning of the fatigue test setup, and an non-destructive test (NDT) was performed and there was no crack.

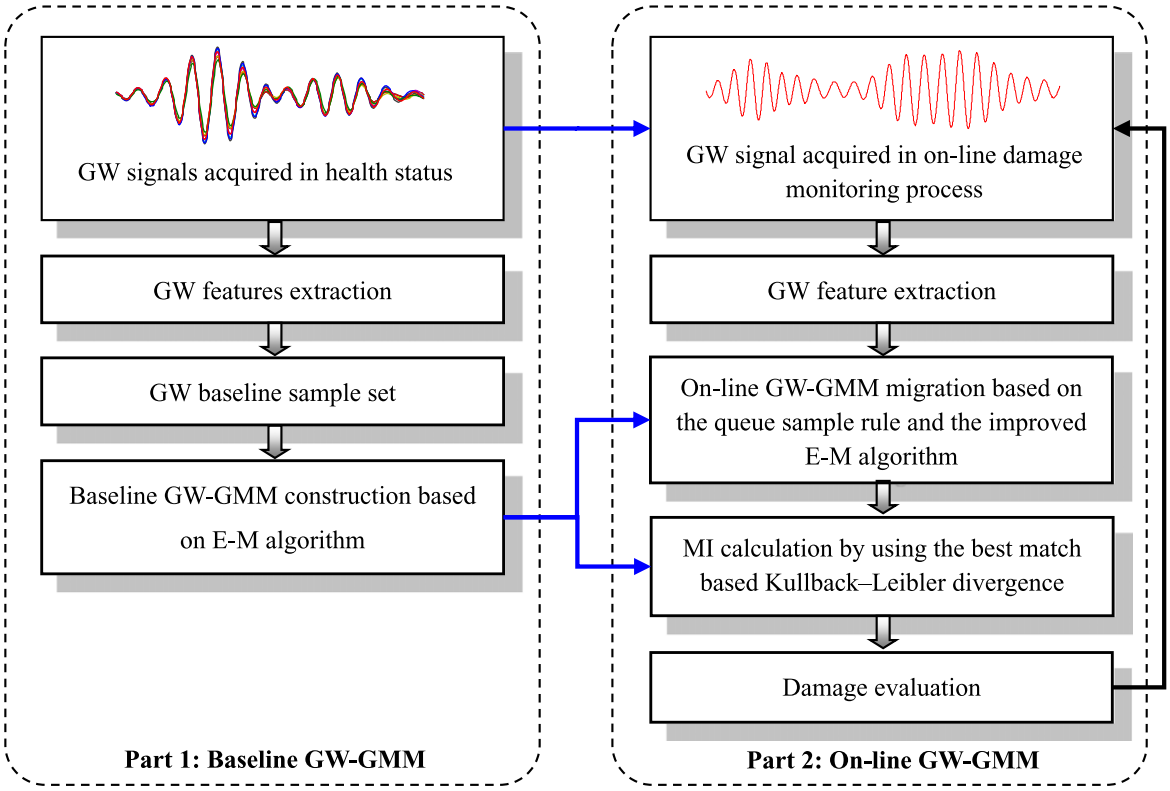

Figure 3. Implementation process of the GW-GMM.

The fatigue test was divided into two phases. Phase 1 was hotspot crack monitoring and phase 2 was crack propagation monitoring. The duration time of phase 1 was totally 125 effective test days and nearly 1000 flight hours were simulated through the fatigue test but there was no crack. At the end of phase 1, a crack was detected at the right landing gear spar by using visual NDT based on an endoscope. This area was not monitored in phase 1. Therefore, phase 2 was decided to be performed to monitor the crack propagation. This area was defined as hotspot 1 and it is shown in figure 4. The fatigue load at hotspot 1 was complicated and the strain level was around -1200 to $1500\,\mu\varepsilon$. The crack length was 33.5 mm when it was detected. Thus two PZT layers were placed on both sides of the crack to construct a GW pitch-catch channel. Though there was a crack, the structure was still supposed to be in the healthy state after the PZT layers were placed on it. In the following fatigue test, the crack propagation must be monitored reliably. In addition, another crack of length 35.1 mm was discovered at the left wing panel in the middle of phase 2. Thus the crack propagation monitoring of this crack area defined as hotspot 2 was also decided to be performed. It is also shown in figure 4. The strain level of hotspot 2 was around -700 to $400\,\mu\varepsilon$. Two PZT layers were placed on both sides of the crack.

The material of the two hotspots is 7B04 super-hardness aluminum alloy and the thickness of the two hotspots is all around 10 mm. The sensor element of the PZT layer is piezoceramic and the type is PZT-5A. The diameter and thickness of the piezoceramic are 8 mm and 0.48 mm respectively. These PZT layers were placed on the structure by using an adhesive of two component epoxy paste. The adhesive type is Araldite® AW 113 with HV 953 K. The adhesive was cured by using a hot air gun for 45 min and the curing temperature was around 60 °C. The distance between the two PZT layers in one hotspot was around 60 mm.

The scanning system was used to control the two GW channels to excite and acquire GW signals. A five-cycle sine burst modulated by Hanning window was adopt to be GW excitation signal [28]. The sampling frequency and excitation amplitude were set to be 10 MSamples s^{-1} and ± 70 V respectively. In order to reduce signal noise, 100 sampling average was adopted.

It should be noted that the excitation frequency of GW signal is an important parameter for the GW based SHM method. Thus, a frequency scanning process, which was from 25 to 500 kHz (10 kHz interval), was performed first to select a proper excitation frequency. To monitor crack propagation, high frequency of GW signal is preferred because of short wavelength. In addition, there was large white noise and low frequency interference in the GW signal. To promise a relative high signal to noise ratio, the GW signal of higher amplitude is preferred. The GW signal is also complicated due to the complex structure. The direct wave of less signal aliasing is preferred to be the signal segment for crack propagation monitoring. Based on these reasons, the GW signal of excitation frequency of 250 kHz is relatively better than that of the other frequencies. Thus 250 kHz is selected to be the excitation frequency of the GW signal in the fatigue test.

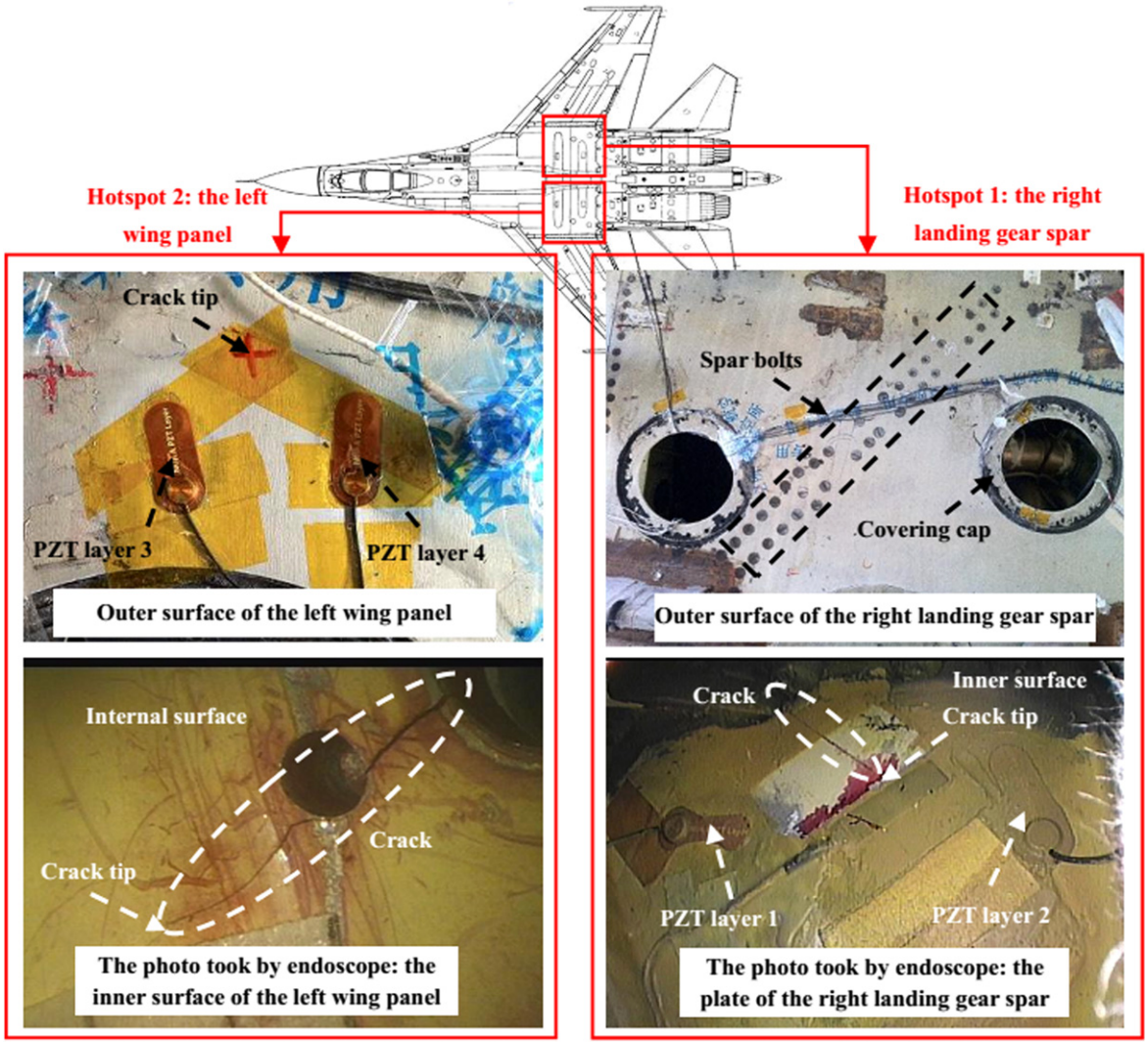

Figure 4. Layout of hotspots for crack propagation monitoring in phase 2.

The duration time of the fatigue test for hotspots 1 and 2 were 24 and 11 effect test days respectively. In each test day, the two hotspots were scanned by using the scanning system in a fixed time interval automatically and 50 GW signals were acquired correspondingly. It should be noted that the acquisition of the GW signals was performed under the fatigue load condition. Totally 1200 GW signals numbered from Signal No. 1 to 1200 were acquired at hotspot 1 and 550 GW signals numbered from Signal No. 1 to 550 were acquired at hotspot 2.

When the fatigue load was unloaded in each test day, the endoscope was used to detect the crack length. The results indicate that the crack propagated 0.35 mm d^{-1} approximately.

3.2. GW signal and time-varying conditions

Due to the large white noise and low frequency interference in the GW signal, a wavelet transform based de-nosing method [28] was adopted to reduce the noise of all the GW signals first.

Two de-noised GW signals acquired at hotspots 1 and 2 are shown in figures 5(a) and (b) respectively. The direct wave of the signal can be distinguished clearly and the peak value of the direct wave is the maximum value of the whole signal. Considering that the crack propagation path was on or near the direct propagation path of the GW, the direct wave and the signal segment of boundary reflections next to the direct wave are emphasized to be the main signal segment for crack propagation monitoring. Thus, the length of the signal segment which is adopted to monitor the crack propagation is from 1.101×10^{-4} to 1.550×10^{-4} s for hotspot 1 and is from 1.051×10^{-4} to 1.500×10^{-4} s for hotspot 2. The crosstalk signal shown in the GW signal was introduced by the scanning system. It can be eliminated by using signal interception.

Environmental temperature is an important time-varying factor for GW [9, 10]. However, as shown in figure 6, the temperature influence can be ignored in the short duration time of the fatigue test of phase 2 because the temperature measuring results show that the average temperature difference in a test day was about 3.5 °C and the average

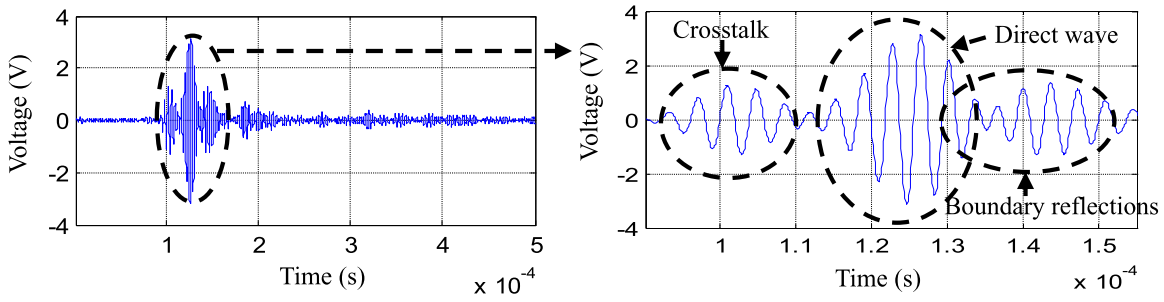

(a) Typical GW signal of hotspot 1

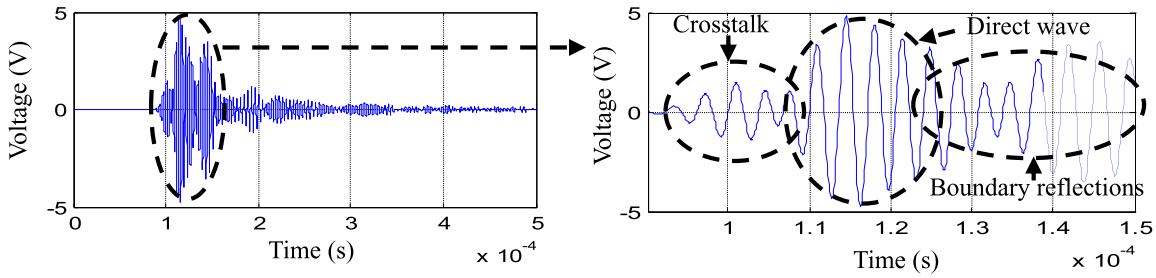

(b) Typical GW signal of hotspot 2

Figure 5. Illustration of the signal segment for crack propagation monitoring.

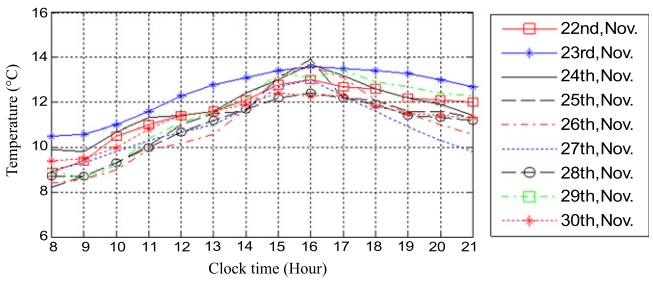

Figure 6. Environmental temperature measured in phase 2.

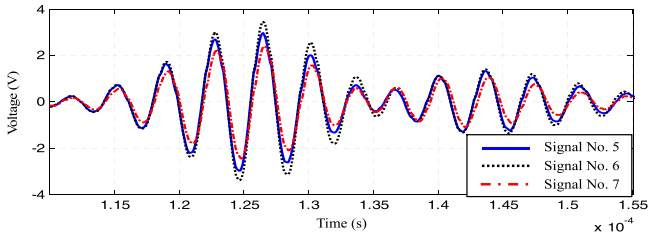

Figure 7. Typical GW signals acquired at hotspot 1 under the fatigue load condition.

temperature difference between different test days was only about 1.7 °C.

Figure 7 gives the Signal No. 5–7 acquired at hotspot 1 in the first test day under the fatigue load condition. The crack propagation influence can be ignored because the three signals were acquired continuously. It can be noted that the fatigue load introduced large variation to the amplitude of these signals and the fatigue load can also affect the time-of-flight (ToF). The method of ToF measurement is an envelope detection method which is based on complex wavelet transform [28]. The repeatability error of the peak value of the three signals is up to 17%. The fatigue load influence at hotspot 2 was lower than that at hotspot 1. The repeatability error of the peak value of hotspot 2 is around 8%. It should be noted that the strain level of hotspot 1 was higher than that of hotspot 2, which means that the uncertainty influence introduced by the fatigue load of hotspot 1 should be higher than that of hotspot 2.

Figure 8 displays all the GW signals acquired at hotspot 1 under the fatigue load condition. It can be seen that the attenuation of the peak value caused by the crack propagation is mixed into the fatigue load influence. The cumulative variation trend of the peak and the TOF can only be noted weakly when the crack propagation length was longer than 4 mm. The crack propagation length of hotspot 2 was shorter than that of hotspot 1. Thus the crack propagation induced cumulative variation trend is hard to be noted, as shown in figure 9.

According to the signal variations shown in figures 8 and 9, it can be said that the main time-varying factors were the fatigue load condition and the corresponding structural boundary changing condition. The fatigue load which was applied to the full-scale structure was based on a fatigue load spectrum of random and dynamic. The fatigue load spectrum was generated by using the in-service flight data to simulate different flight modes of the aircraft such as takeoff, level flight, overloading, landing, on-ground etc. In each test day, the GW signals were acquired in a fixed time interval automatically under fatigue loading condition. Thus the GW signals should cover a wide range of different fatigue load states and different crack states such as open crack and closed crack, etc. The aim of the GW-GMM is to realize the crack propagation monitoring under these situations.

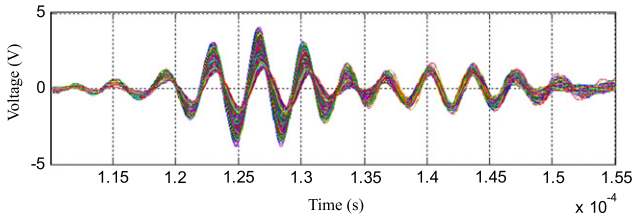

(a) GW Signals

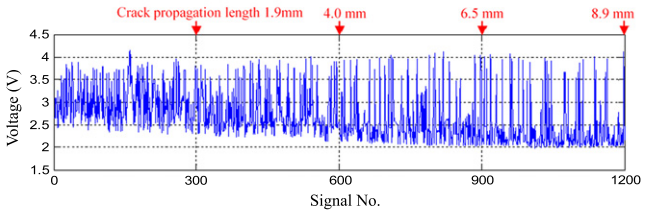

(b) Peak value of the GW signals

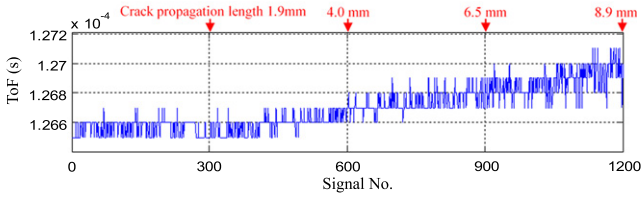

(c) ToF of the GW signals

Figure 8. GW signals acquired at hotspot 1.

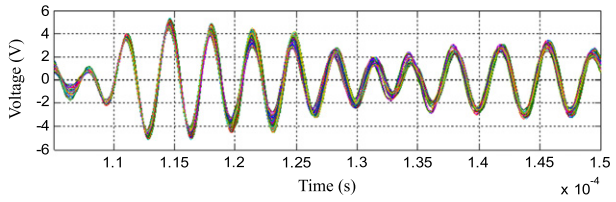

(a) GW Signals

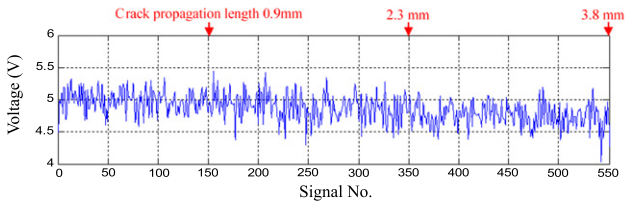

(b) Peak value of the GW signals

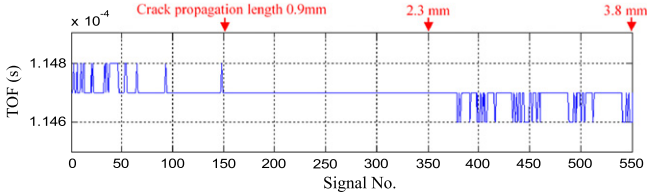

(c) ToF of the GW signals

Figure 9. GW signals acquired at hotspot 2.

3.3. GW feature extraction and the time-varying influence

For crack propagation monitoring by using only one GW channel, DI [26] is often used. In this paper, the following two DI, but not limited, are adopted to extract GW feature.

(1) DI_1 is the time domain cross-correlation shown in equation (11). The motivation of using this DI is that it is mainly affected by the changes of signal waveform shape or signal ToF

$$DI_1 = 1 - \sqrt{\frac{\left\{\int_{t_0}^{t_1} \boldsymbol{b}(t)\boldsymbol{m}(t)\mathrm{d}t\right\}^2}{\left\{\int_{t_0}^{t_1} \boldsymbol{b}^2(t)\mathrm{d}t \int_{t_0}^{t_1} \boldsymbol{m}^2(t)\mathrm{d}t\right\}}}, \tag{11}$$

where, $\boldsymbol{b}(t)$ and $\boldsymbol{m}(t)$ represent baseline signal and monitoring signal respectively. t_0 and t_1 are the start and stop time corresponding to the selected signal segment. The scale of DI_1 is [0, 1].

(2) DI_2 is the magnitude difference of frequency response shown in equation (12). This DI is mainly affected by the changes of signal amplitude or signal energy

$$DI_2 = \sqrt{\frac{\int_{\omega_0}^{\omega_1} (|\boldsymbol{b}(\omega)| - |\boldsymbol{m}(\omega)|)^2\mathrm{d}\omega}{\int_{\omega_0}^{\omega_1} |\boldsymbol{b}(\omega)|^2\mathrm{d}\omega}}, \tag{12}$$

where $\boldsymbol{b}(\omega) = \int_{t_0}^{t_1} \boldsymbol{b}(t)\mathrm{e}^{-\mathrm{j}\omega t}\mathrm{d}t$ and $\boldsymbol{m}(\omega) = \int_{t_0}^{t_1} \boldsymbol{m}(t)\mathrm{e}^{-\mathrm{j}\omega t}\mathrm{d}t$. $|\cdot|$ denotes the modules value of the frequency response. ω_0 and ω_1 are the start and stop frequency corresponding to the selected frequency spectrum window. The start and stop of the frequency spectrum window are selected to be 150 kHz and 350 kHz respectively. The variation range of DI_2 is also [0, 1].

For hotspot 1, DI_1 and DI_2 calculated by using the Signal No. 1 as the baseline signal and all the 1200 GW signals as the monitoring signals are given in figure 10. They appear a cumulative increasing trend when the crack propagation length was longer than 4 mm. However, the early stage of the crack propagation is hard to be recognized because of the random variations introduced by time-varying conditions.

For hotspot 2, DI_1 and DI_2 are shown in figure 11. In this hotspot, the crack propagation was at the early stage. Comparing figure 11 with 10, the influence of time-varying conditions was lower in hotspot 2. Therefore, a cumulative increasing trend was appeared weakly in figure 11.

In conventional DI based damage monitoring methods, a DI threshold is often predefined. When the value of the DI exceeds the threshold, the damage occurrence can be determined. However, the threshold is hard to be determined based on the results and the crack propagation monitoring is also difficult to be realized, especially at the early stage of the crack propagation.

4. Crack propagation monitoring based on the GW-GMM

In this section, the GW feature sample set is discussed first. Then, the baseline GW-GMM and the migration process of

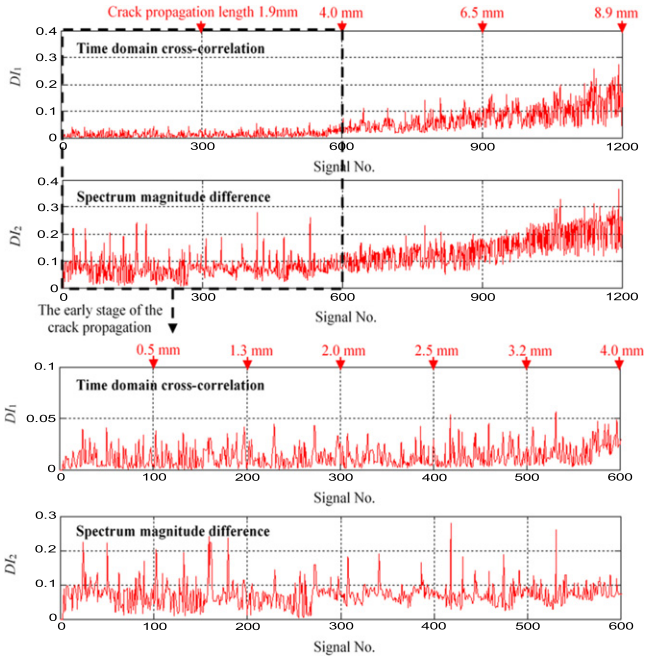

Figure 10. Damage indexes of hotspot 1.

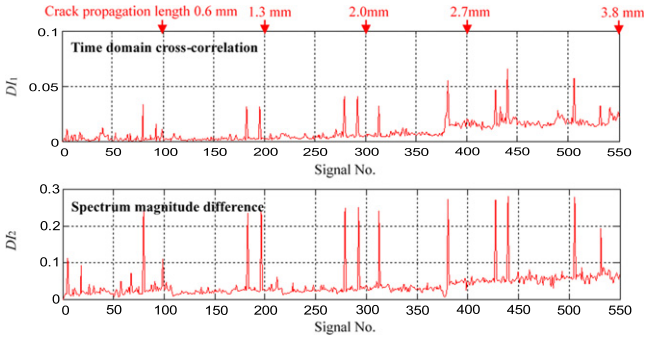

Figure 11. Damage indexes of hotspot 2.

the on-line GW-GMM is given. After that, the crack propagation monitoring results by using the GW-GMM are given and discussed.

4.1. GW feature sample set

To improve the reliability of crack propagation monitoring in the full-scale aircraft fatigue test, the GW-GMM is applied to the GW signals mentioned above. For hotspot 1, the GW signals numbered from Signal No. 1 to 600 which belongs to the early stage of the crack propagation are adopted. Totally 600 GW features are obtained by using the Signal No. 1 to be the baseline signal and all the 600 signals to be monitoring signals. For hotspot 2, all the GW signals are used and totally 550 GW features are obtained. All the GW features are shown in figure 12. It can be noted from figure 12(a) that the GW features of hotspot 1 of different crack propagation length are overlapped seriously and appear a weak cumulative variation trend. Different from hotspot 1, the GW features of hotspot 2 shown in figure 12(b) appear a slow cumulative variation trend.

4.2. GW-GMM construction and migration

For hotspot 1, the first 50 GW features belonged to the first test day are used as GW baseline sample set to construct a baseline GW-GMM at the first part shown in figure 3. All the 600 GW features are input to the second part one by one to calculate the MI. For hotspot 2, the first 50 feature vectors are also adopted to construct a baseline GW-GMM. All the 550 features are used to calculate the MI. Although the first 50 GW features are adopted to construct the baseline GW-GMM, they can be still adopted to validate the migration process of the GW-GMM. The length of the feature sample set is $K = 50$.

An important step of the GW-GMM is to determine the number of Gaussian components before it is implemented. Indeed, the more Gaussian components are used, the higher sensitivity it may be reached. However, the sensitivity also depends on the spread of the GW features. In addition, the computational efficiency and the GMM stability will be reduced by using so many Gaussian components. If few Gaussian component is used, an average effect will be appeared so as to reduce the sensitivity [37–40]. For hotspot 1, the number of Gaussian components is set to be 3 to cover the GW feature sample set. For hotspot 2, the number of Gaussian components is set to be 2. One is used to cover the concentrated GW features and the other is used to cover the dispersed GW features. The baseline GW-GMM of the two hotspots are shown in figures 13(a) and 14(a) respectively.

For on-line migration of the GW-GMM, the correction factor shown in equation (6) is set to be 1×10^{-3} considering the scale of the GW features is [0, 1]. Based on the migration method, some typical on-line migrated GW-GMMs of the two hotspots accompanying with the crack propagation are shown in figures 13(a)–(c) and 14(a)–(c) respectively.

For hotspot 1, the Gaussian components Φ_1 and Φ_2 move slowly to track the relative concentrated GW features and the Gaussian component Φ_3 moves fast to track the relative dispersed GW features. At the early stage of the crack propagation monitoring, the mixture probability of the on-line GW-GMM shown in figure 13(b) is similar to that of the baseline GW-GMM shown in figure 13(a). This is because that the GW features are overlapped in high degree at this stage. When the crack propagation length was increased and the GW features are accumulated, the on-line GW-GMM is migrated thoroughly as shown in figures 13(c) and (d). The result indicates that the weak cumulative variation trend of the GW feature sample set is enlarged by the fast changing of the mixture probability of the on-line GW-GMM.

For hotspot 2, the Gaussian component Φ_1 moves slowly to track the concentrated GW features and the Gaussian component Φ_2 moves fast to track the dispersed GW features as shown in figure 14. It can be noted by comparing the four GW-GMMs that the Gaussian component Φ_1 shows a cumulative migration trend and the Gaussian component Φ_2 shows a fast migration trend.

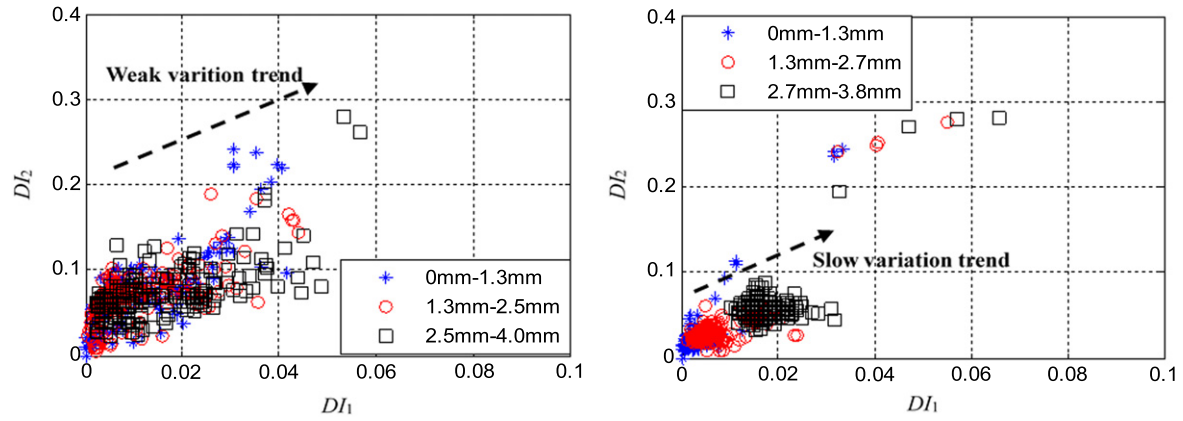

(a) Sample set of hotspot 1 (b) Sample set of hotspot 2

Figure 12. GW Feature sample set.

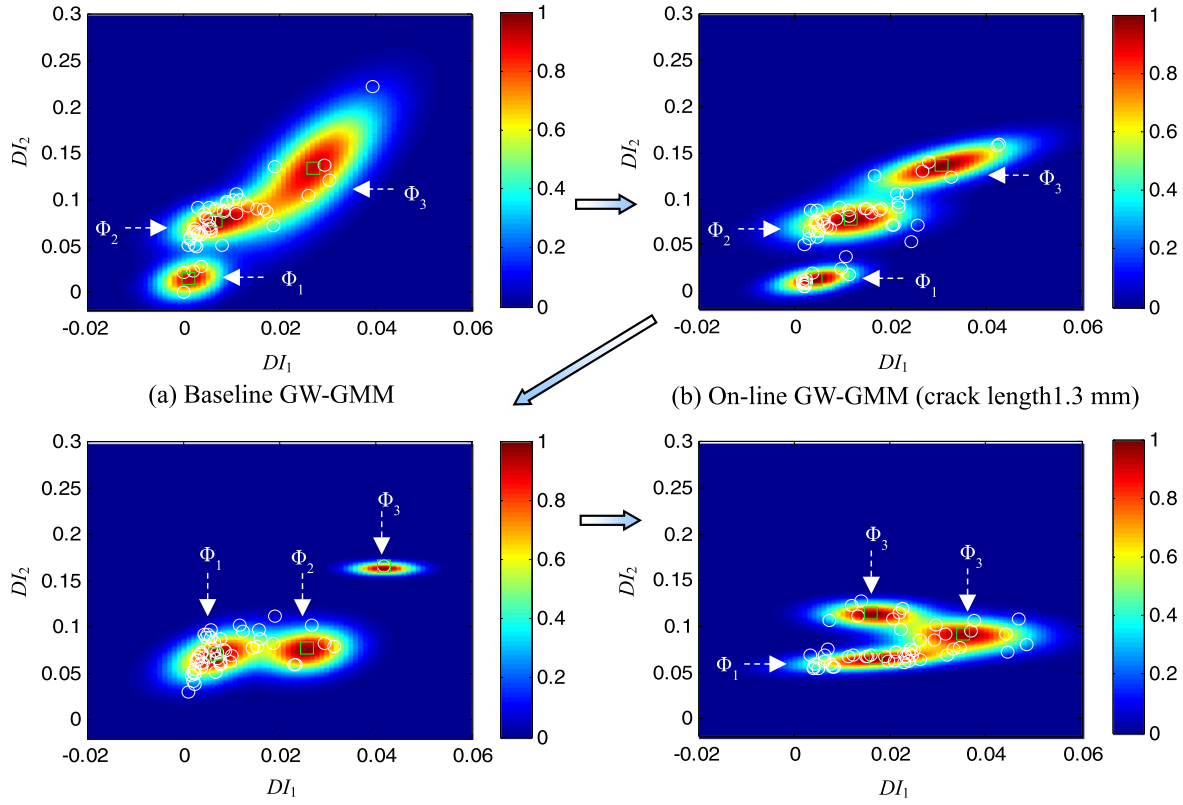

(a) Baseline GW-GMM (b) On-line GW-GMM (crack length1.3 mm)

(c) On-line GW-GMM (crack length 2.5 mm) (d) On-line GW-GMM (crack length 4.0 mm)

Figure 13. GW-GMM migration process of hotspot 1.

4.3. Crack propagation monitoring results

The crack propagation monitoring results of the two hotspots are shown in figure 15. As it can be seen that the MI corresponding to the first 50 GW features approach zero, which means that the variation property of these GW features has been completely contained in the baseline GW-GMM.

For hotspot 1, the MI are increased slowly from the crack length 0.5–2 mm because the GW features are overlapped in high degree. The MI are increased prominently from the crack length 2.0 to 2.5 mm, because the GW-GMM is migrated thoroughly as shown in figures 13(c) and (d).

For hotspot 2, The MI are increased fast and stably because the dispersed GW features is fast tracked by Gaussian component Φ_2 as mentioned above. The MI are also increased faster than that of hotspot 1 because of the lower fatigue load influence.

Compared to the DI shown in figures 10 and 11, it can be known that the MI are increased cumulatively and stably accompanying with the crack propagation. When the crack propagation length is larger than 2 mm, the MI are increased fast. Therefore, the early stage of the crack propagation can be reliably evaluated based on the cumulative increasing trend of the MI.

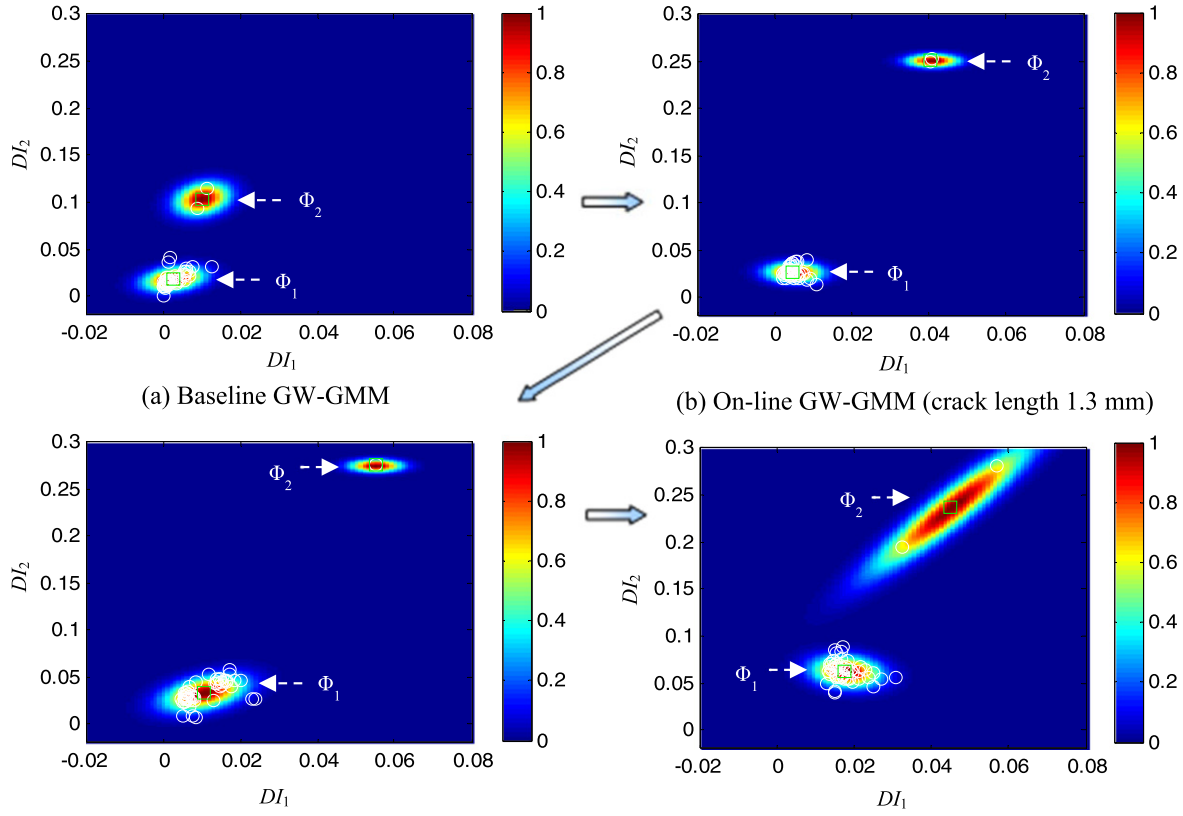

Figure 14. GW-GMM migration process of hotspot 2.

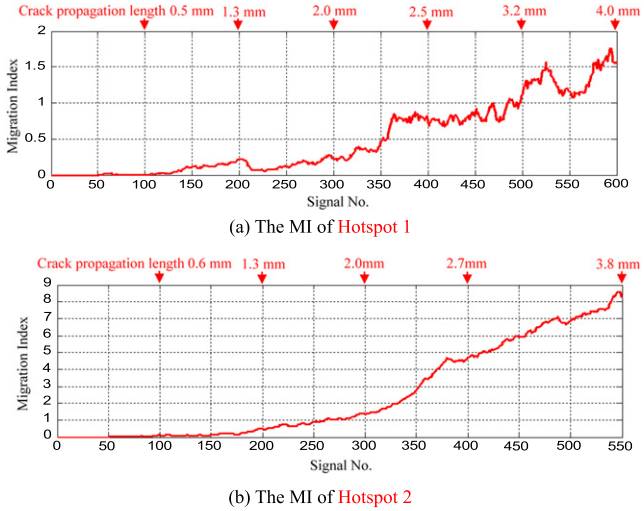

Figure 15. Crack propagation monitoring results based on the GW-GMM.

5. Conclusion

The GW based SHM method is applied to a full-scale aircraft fatigue test. The GW-GMM method is proposed to improve the crack propagation monitoring reliability under time-vary conditions, especially at the early stage of the crack propagation. The monitoring results in the full-scale aircraft fatigue test show a high performance of the GW-GMM. However, there are several further studies will be performed in the near future to improve the GW-GMM. They are given as follows.

(1) The feature extracting methods of GW signal in time domain, frequency domain and time–frequency domain [43–49] will be systematically studied to reduce the spread of the GW features and thus to increase the crack monitoring sensitivity.
(2) As mentioned before, an important step of the GW-GMM is to determine the number of Gaussian components. To take this problem into account, an adaptive GW-GMM method will be studied, in which the number of Gaussian components can be changed adaptively and automatically.
(3) The environmental influence such as temperature is low in the fatigue test. More full-scale aircraft fatigue tests will be performed in the near future to validate the GW-GMM under a more comprehensive time-varying condition.

Acknowledgments

The authors would like to acknowledge the Beijing Aeronautical Technology Research Center of China to supply the full-scale fatigue test. This work is also sponsored by the National Science Fund for Distinguished Young Scholars

(Grant No. 51225502), the National Natural Science Foundation of China (Grant No. 51575263), the Fundamental Research Funds for the Central Universities (Grant No. NE2016001), the Priority Academic Program Development of Jiangsu Higher Education Institutions and the Qing Lan Project.

References

[1] McCollom N N and Brown E R 2011 PHM on the F-35 fighter *IEEE Conf. on Prognostics and Health Management (PHM) (Montreal Canada)* pp 1–10
[2] Esperon-Miguez M, John P and Jennions I K 2013 A review of integrated vehicle health management tools for legacy platforms: challenges and opportunities *Prog. Aerosp. Sci.* **56** 19–34
[3] Boller C, Chang F K and Fujino Y 2009 *Encyclopedia of Structural Health Monitoring* (New York: Wiley)
[4] Staszewski W J, Mahzan S and Traynor R 2009 Health monitoring of aerospace composite structures active and passive approach *Compos. Sci. Technol.* **69** 1678–85
[5] SAE international 2013 *Guidelines for Implementation of Structural Health Monitoring on Fixed Wing Aircraft* ARP6461 SAE International
[6] Buderath M, McFeat J and Azzam H 2014 The need for guidance on integrating structural health monitoring within military aircraft systems *Struct. Health Monit.* **13** 581–90
[7] Lopez I and Sarigul-Klijn N 2010 A review of uncertainty in flight vehicle structural damage monitoring, diagnosis and control: challenges and opportunities *Prog. Aerosp. Sci.* **46** 247–73
[8] Schubert K J, Brauner C and Hermann A 2014 Non-damage related influences on Lamb wave based SHM of CFRP structures *Struct. Health Monit.* **13** 158–76
[9] Croxford A J, Moll J, Wilcox P D and Michaels J E 2010 Efficient temperature compensation strategies for guided wave structural health monitoring *Ultrasonics* **50** 517–28
[10] Roy S, Lonkar K, Janapati V and Chang F K 2104 A novel physics-based temperature compensation model for structural health monitoring using ultrasonic guided waves *Struct. Health Monit.* **13** 321–42
[11] Lim H J, Sohn H, DeSimio M P and Brown K 2014 Reference-free fatigue crack detection using nonlinear ultrasonic modulation under various temperature and loading conditions *Mech. Syst. Signal Process.* **45** 468–78
[12] Su Z Q, Zhou C, Hong M, Cheng L, Wang Q and Qing X L 2014 Acousto-ultrasonics-based fatigue damage characterization: linear versus nonlinear signal features *Mech. Syst. Signal Process.* **45** 225–39
[13] Figueiredo E, Park G, Farrar C R, Worden K and Figueiras J 2011 Machine learning algorithms for damage detection under operational and environmental variability *Struct. Health Monit.* **10** 559–72
[14] Worden K, Cross E J, Antoniadou I and Kyprianou A 2014 A multiresolution approach to cointegration for enhanced SHM of structures under varying conditions—an exploratory study *Mech. Syst. Signal Process.* **47** 243–62
[15] Lapira E, Brisset D, Ardakani H D, Siegel D and Lee J 2012 Wind turbine performance assessment using multi-regime modeling approach *Renew. Energy* **45** 86–95
[16] Dong Y L, Fang F and Gu Y J 2013 Dynamic evaluation of wind turbine health condition based on Gaussian mixture model and evidential reasoning *J. Renew. Sustain. Energy* **5** 033117
[17] Heyns T, Heyns P S and De Villiers J P 2012 Combining synchronous averaging with a Gaussian mixture model novelty detection scheme for vibration-based condition monitoring of a gearbox *Mech. Syst. Signal Process.* **32** 200–15
[18] Tschope C and Wolff M 2009 Statistical classifiers for structural health monitoring *IEEE Sensors J.* **9** 1567–76
[19] Banerjee S, Qing X L, Beard S and Chang F K 2010 Prediction of progressive damage state at the hot spots using statistical estimation *J. Intell. Mater. Syst. Struct.* **21** 595–605
[20] Qiu L, Yuan S F, Chang F K, Bao Q and Mei H F 2014 On-line updating Gaussian mixture model for aircraft wing spar damage evaluation under time-varying boundary condition *Smart Mater. Struct.* **23** 125001
[21] Chakraborty D, Kovvali N, Papandreou-Suppappola A and Chattopadhyay A 2015 An adaptive learning damage estimation method for structural health monitoring *J. Intell. Mater. Syst. Struct.* **26** 125–43
[22] Dragan K, Dziendzikowski M, Uhl T and Stepinski T 2014 Remote monitoring of fatigue cracks growth in the aircraft structure based on active piezosensor network during the full scale fatigue test *Key Eng. Mater.* **588** 249–56
[23] Su Z, Yang C, Pan N, Ye L and Zhou L M 2007 Assessment of delamination in composite beams using shear horizontal (SH) wave mode *Compos. Sci. Technol.* **67** 244–51
[24] Ihn J B and Chang F K 2008 Pitch-catch active sensing methods in structural health monitoring for aircraft structures *Struct. Health Monit.* **7** 5–19
[25] Qing X L, Beard S, Shen S B, Bradley I, Salama M M and Chang F K 2009 Development of a real-time active pipeline integrity detection system *Smart Mater. Struct.* **18** 115010
[26] Su Z and Ye L 2009 *Identification of Damage using Lamb Waves: From Fundamentals to Applications* (Berlin: Springer)
[27] Yu L, Bottai-Santoni G and Giurgiutiu V 2010 Shear lag solution for tuning ultrasonic piezoelectric wafer active sensors with applications to Lamb wave array imaging *Int. J. Eng. Sci.* **48** 848–61
[28] Qiu L, Liu M L, Qing X L and Yuan S F 2013 A quantitative multi-damage monitoring method for large-scale complex composite *Struct. Health Monit.* **12** 183–96
[29] Jarmer G, Flynn E and Todd M D 2013 Multi-wave-mode, multi-frequency detectors for guided wave interrogation of plate structures *Struct. Health Monit.* **13** 120–30
[30] Zhou W, Li H and Yuan F G 2014 Guided wave generation, sensing and damage detection using in-plane shear piezoelectric wafers *Smart Mater. Struct.* **23** 015014
[31] Wu Z J, Liu K H, Wang Y S and Zheng Y B 2014 Validation and evaluation of damage identification using probability-based diagnostic imaging on a stiffened composite panel *J. Intell. Mater. Syst. Struct.* **26** 2181–95
[32] Sharif-Khodaei Z and Aliabadi M H 2014 Assessment of delay-and-sum algorithms for damage detection in aluminium and composite plates *Smart Mater. Struct.* **23** 075007
[33] Wu W L, Qu W Z, Xiao L and Inman D J 2015 Detection and localization of fatigue crack with nonlinear instantaneous baseline *J. Intell. Mater. Syst. Struct.* (doi:10.1177/1045389X15596851)
[34] Wandowski T, Malinowski P H and Ostachowicz W M 2015 Circular sensing networks for guided waves based structural health monitoring *Mech. Syst. Signal Process.* **66-67** 248–67
[35] Hall J S and Michaels J E 2015 Multipath ultrasonic guided wave imaging in complex structures *Struct. Health Monit.* **14** 345–58
[36] Hong M, Su Z, Lu Y, Sohn H and Qing X L 2015 Locating fatigue damage using temporal signal features of nonlinear Lamb waves *Mech. Syst. Signal Process.* **60** 182–97
[37] Dempster A P, Laird N M and Rubin D B 1977 Maximum likelihood from incomplete data via the EM algorithm *J. R. Stat. Soc.* B **39** 1–38

[38] Banfield J D and Raftery A E 1993 Model-based Gaussian and non-Gaussian clustering *Biometrics* **49** 803–21
[39] Ormoneit D and Tresp V 1995 Improved Gaussian mixture density estimates using Bayesian penalty terms and network averaging *9th Annual Conf. NIPS (Denver, CO)* vol 8 pp 542–8
[40] Goldberger J, Gordon S and Greenspan H 2003 An efficient image similarity measure based on approximations of KL–Divergence between two Gaussian mixtures *Proc. 9th IEEE Int. Conf. on Computer Vision (Nice, France)* vol 1 pp 487–93
[41] Qiu L, Yuan S F, Shi X L and Huang T X 2012 Design of piezoelectric transducer layer with electromagnetic shielding and high connection reliability *Smart Mater. Struct.* **21** 075032
[42] Qiu L and Yuan S F 2009 On development of a multi-channel PZT array scanning system and its evaluating application on UAV wing box *Sensors Actuators* A **151** 220–30
[43] Konstantinidis G, Drinkwater B W and Wilcox P D 2006 The temperature stability of guided wave structural health monitoring systems *Smart Mater. Struct.* **15** 967–76
[44] Li F, Su Z, Ye L and Meng G 2006 A correlation filtering-based matching pursuit (CF-MP) for damage identification using lamb waves *Smart Mater. Struct.* **15** 1585–94
[45] Lu Y, Ye L, Su Z, Zhang L and Cheng L 2008 Artificial neural network (ANN)-based crack identification in aluminum plates with lamb wave signals *J. Intell. Mater. Syst. Struct.* **20** 39–49
[46] Lu Y H and Michaels J E 2009 Feature extraction and sensor fusion for ultrasonic structural health monitoring under changing environmental conditions *IEEE Sensors J.* **9** 1462–71
[47] Zhou C, Hong M, Su Z, Wang Q and Cheng L 2012 Evaluation of fatigue cracks using nonlinearities of acousto-ultrasonic waves acquired by an active sensor network *Smart Mater. Struct.* **22** 015018
[48] Quaegebeur N, Ostiguy P C and Masson P 2014 Correlation-based imaging technique for fatigue monitoring of riveted lap-joint structure *Smart Mater. Struct.* **23** 055007
[49] Torkamani S, Roy S, Barkey M E, Sazonov E and Kotru S 2014 A novel damage index for damage identification using guided waves with application in laminated composites *Smart Mater. Struct.* **23** 095015